

Investigation of chromophore-chromophore interaction by electro-optic measurements, linear dichroism, x-ray scattering, and density-functional calculations

D. Apitz,^{1,2,*} R. P. Bertram,² N. Benter,² W. Hieringer,³ J. W. Andreasen,⁴ M. M. Nielsen,⁴ P. M. Johansen,⁵ and K. Buse²

¹*Optics and Plasma Research Department, Risø National Laboratory, 4000 Roskilde, Denmark*

²*Institute of Physics, University of Bonn, 53115 Bonn, Germany*

³*Department of Physical and Theoretical Chemistry, Friedrich-Alexander-University Erlangen-Nuremberg, 91058 Erlangen, Germany*

⁴*Danish Polymer Center, Risø National Laboratory, 4000 Roskilde, Denmark*

⁵*SIMAC - Svendborg International Maritime Academy, 5700 Svendborg, Denmark*

(Received 9 February 2005; published 14 September 2005)

Free-beam interferometry and angle-resolved absorption spectra are used to investigate the linear electro-optic coefficients and the linear dichroism in photoaddressable bis-azo copolymer thin films. From the first- and second order parameters deduced, the chromophore orientation distribution is calculated and displayed for several poling temperatures and chromophore concentrations. The influence of dipole-dipole interaction on the overall polymer dynamics is discussed. The first order parameter, and therefore the Pockels effect, peaks for a poling temperature of around 10 °C above the glass transition. The decrease of the Pockels effect above this temperature region is triggered by a head-to-tail chromophore orientation, i.e., a transition to a microcrystalline phase, increasing the second order parameter. Comparison of the experimentally observed absorption spectra and those obtained by density-functional calculations support the picture of differently aligned bis-azo dye molecules in a *trans,trans* configuration. Complementary wide-angle x-ray scattering is recorded to confirm the various kinds of ordering in samples poled at different temperatures.

DOI: [10.1103/PhysRevE.72.036610](https://doi.org/10.1103/PhysRevE.72.036610)

PACS number(s): 42.70.Jk, 82.35.Ej, 61.10.Eq, 71.15.Mb

I. INTRODUCTION

During the last years the flexibility and promising material parameters of polymers have motivated investigations of how they may be integrated into technical applications. For example, the linear electro-optic response yields larger efficiencies than in conventional crystalline materials and electro-optic modulation in polymers was shown to reach as far as the terahertz range [1], far beyond what crystals are capable of due to the existence of phonons. However, even though the material properties in focus have been discovered several decades ago, a broad exploitation has not yet occurred.

In order to use polymers, for many applications a specific structure has to be generated in the material, such as an optically written volume grating or an electrically induced break of the inversion symmetry. Disordered materials have, of course, no melting point, but exhibit a glass transition temperature, causing dynamics to take place at all temperatures. When considered for technical application, temperature stability is often the most crucial characteristic feature. Usually, extrapolations of experiments at higher temperatures are performed to gain this kind of information. As an example, telecommunication devices are required to pass stability tests at 85 °C for several weeks [2]. In addition to this experimental approach, there is an ongoing effort to describe mathematically the dynamics of electro-optic dipolar molecules immersed into a polymer matrix. Interactions of these chromophores with an external field or molecular surroundings of the matrix have been modeled to predict and explain polymer dynamics [3–6]. However, so far dipole-dipole in-

teraction has not been taken into account, even though a strong interaction is known from cooperative movements in polymers with high chromophore concentration [7]. It is not fully understood how chromophore-chromophore interaction and the dynamics in polymeric materials can be described efficiently in practice.

In this paper, free beam electro-optic interferometry and linear dichroism measurements are combined to obtain the first, second, and third order parameters and to calculate the chromophore orientation distribution for several poling temperatures and chromophore concentrations. In order to do so, the second-order electro-optic coefficients and the angle-resolved absorption spectra in photoaddressable bis-azo copolymer thin films are measured. Density-functional calculations have been carried out on representative bis-azo monomers in a *trans,trans* configuration, in a *cis,trans* configuration, and in a *trans,cis* configuration to compare calculated absorption spectra with those obtained experimentally. Subsequently, these calculations on parallel and antiparallel aligned *trans,trans* molecules (head-to-head and head-to-tail orientation) allow us to study the influence of chromophore-chromophore interactions on absorption spectra and orientation dynamics. The partial order of the chromophores is then confirmed with grazing incidence wide-angle x-ray scattering.

II. ORIENTATION DISTRIBUTION FUNCTION

In order to describe the dynamics of nonlinear chromophores, a time-dependent orientation distribution function $g(\theta, \phi, t)$ of the orientation solid angles of these dipoles immersed into a polymer matrix is introduced [3,6]. Normalization requires that

*Email address: dirk.apitz@risoe.dk

$$\int_0^{2\pi} \int_0^\pi g(\theta, \phi, t) \sin \theta d\theta d\phi = 1. \quad (1)$$

In a disordered poled or unpoled material, this distribution reduces to $g(\theta, t)$, because of having a rotational symmetry with the axis that points along the direction of the externally applied electric field. Furthermore, far below the glass transition temperature, the distribution can be considered to be independent of time t . Due to the symmetry, it is convenient to expand the distribution function in terms of Legendre polynomials P_n

$$g(\theta) = \sum_{n=0}^{\infty} \frac{i_n}{i_0} \frac{2n+1}{2} P_n(\cos \theta), \quad (2)$$

where the i_n are the spherical modified Bessel functions [3]. The order parameters $a_n = i_n/i_0$ can be introduced and obtained by averaging the n th Legendre polynomials,

$$P_0(\cos \theta) = 1,$$

$$P_1(\cos \theta) = \cos \theta,$$

$$P_2(\cos \theta) = \frac{1}{2}(3 \cos^2 \theta - 1),$$

$$P_3(\cos \theta) = \frac{1}{2}(5 \cos^3 \theta - 3 \cos \theta), \quad (3)$$

over the entire solid angle with respect to the orientation of the chromophores,

$$a_n = \int_0^{2\pi} \int_0^\pi P_n(\cos \theta) g(\theta) \sin \theta d\theta d\phi = \langle P_n(\cos \theta) \rangle. \quad (4)$$

The first order parameter range, of course, from -1 to 1 and those of the second order parameter are from -0.5 to 1 .

A. First and third order parameter

Considering a glassy polymer with rodlike nonlinear optical molecules having a dominant hyperpolarizability along the z axis of the molecules β_{zzz} and restricting the discussion to the linear electro-optic effect (Pockels effect, second-order nonlinear electro-optic process), the induced microscopic polarization is given by

$$p_z^\omega = \beta_{zzz} E_z^\omega E_z^0, \quad (5)$$

where E_z^ω and E_z^0 are the electric field components in the z direction of the light wave with the frequency ω and the externally applied dc field, respectively.

Integrating the orientation distribution of the molecular polarizations with the optical field parallel or perpendicular to the externally applied dc field leads to two components of the macroscopic polarization. From these relations the electro-optic susceptibility can be obtained as [3]

$$\chi_{333}^{(2)} = fN\beta_{zzz} \langle \cos^3 \theta \rangle \quad \text{and} \quad (6)$$

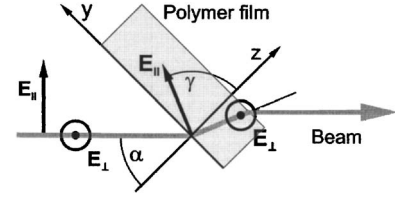


FIG. 1. Schematic representation of the experimental setup for the measurement of linear dichroism.

$$\chi_{113}^{(2)} = fN\beta_{zzz} \frac{1}{2} (\langle \cos \theta \rangle - \langle \cos^3 \theta \rangle), \quad (7)$$

where N is the chromophore density and $\langle \cos \theta \rangle$ the averaged cosine. The local field factor f is added. Its use has been discussed controversially [6] and it has been described for regular crystal lattices by the Lorentz law as $f = (\epsilon_{33} + 2)/3$. However, it also proved to be a good approximation for experimental systems consisting of dipolar molecules [8,9].

If birefringence is neglected, the Pockels coefficients can be written as [10]

$$r_{ijk} = -\frac{2\chi_{ijk}^{(2)}}{n^4}. \quad (8)$$

Contracting the first two indices and using Eqs. (3)–(7), one can calculate the order parameters from the measured Pockels coefficients to be

$$a_1 = -\frac{n^4}{2fN\beta_{zzz}} (2r_{13} + r_{33}) \quad \text{and} \quad (9)$$

$$a_3 = \frac{n^4}{2fN\beta_{zzz}} (3r_{13} - r_{33}). \quad (10)$$

B. Second order parameter

Optical properties that are anisotropic, but inversion symmetric, such as birefringence or linear dichroism (anisotropic absorption), do not require a nonvanishing first order parameter. Considering a material with an anisotropic, rotational symmetric distribution $g(\theta, t)$ of anisotropically absorbing chromophores, a linearly polarized beam with the electric field vector parallel to the symmetry axis is consequently absorbed differently than one with a polarization perpendicular to it. In the case of a polymer film (with the symmetry axis being the film normal z) tilted at an angle of α with respect to an incident laser beam, perpendicularly polarized light (with respect to the incident plane) has the electric field vector completely in the film plane and is subject to the absorption A_\perp (see Fig. 1). Parallel polarized light has the electric field vector at an internal angle of $\gamma = \pi/2 - \arcsin(\sin \alpha/n)$ with respect to the film normal and experiences a different absorption A_\parallel due to the out-of-plane component of the electric field vector. For the described constellation the second order parameter can be determined using the following expression for the dichroic ratio [11]:

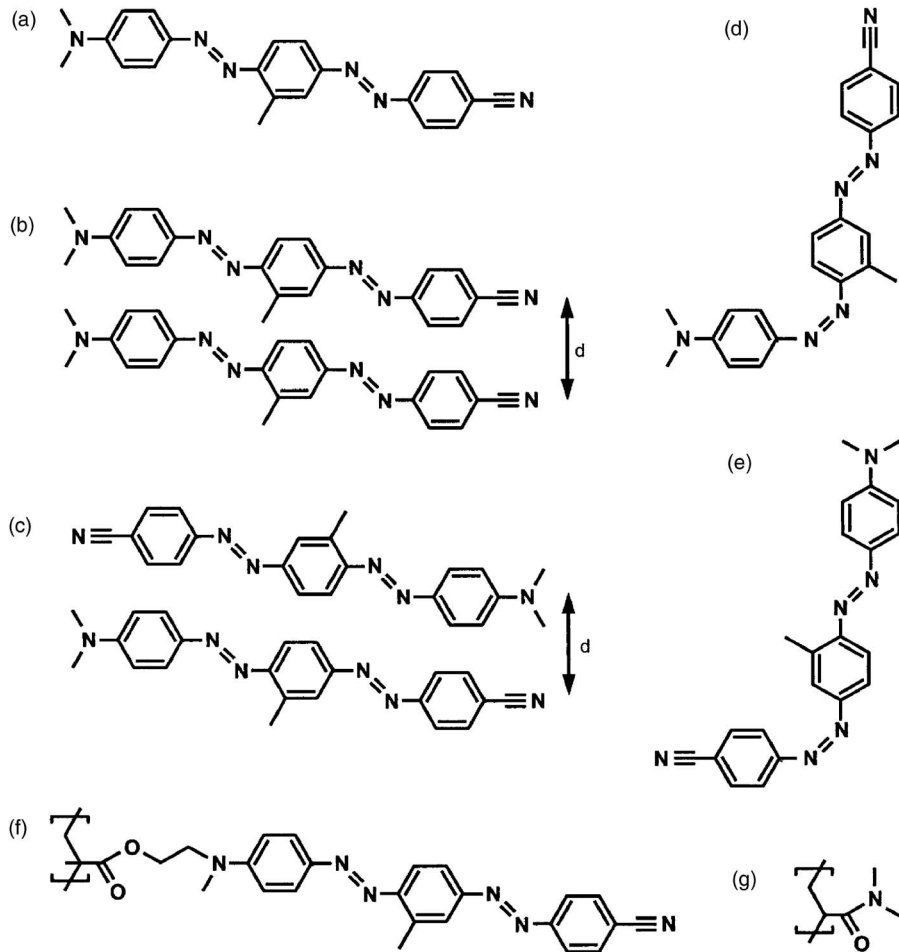


FIG. 2. Chemical structures of chromophore monomers used for computation in a *trans,trans* configuration (a) schematically of their relative positions with the distance d between parallel molecular planes in parallel (b) and antiparallel (c) orientation, of monomers in a *cis,trans* configuration (d) and in a *trans,cis* configuration (e), and of the polymers used for experiment [statistical compositions of the units (f) and (g)].

$$R = \frac{A_{\parallel}}{A_{\perp}} = 1 + \frac{3\langle P_2 \rangle}{(1 - \langle P_2 \rangle)n^2} \cos^2 \gamma, \quad (11)$$

the derivation of which can be found in Ref. [12]. Here, n is the material refractive index. Typically, an anisotropic absorption most generally also requires an anisotropic refractive index. Thus, Eq. (11) is, of course, not strictly true, because the system is presumed to be uniaxially anisotropic. However, Johansson *et al.* gives a detailed calculation with the inclusion of the difference in the refractive indices, which makes the calculation incomparably more tedious, and he proves the expression to be applicable even for lipidic membranes [13,14]. Estimating the deviation not to exceed a few percent, this first approximation gives the possibility for at least qualitative conclusions, which is the reason why, in this paper, birefringence is neglected for simplicity. When restricting our experiments to a constant external angle $\alpha = \pi/4$, the order parameter can, with Eqs. (3), (4), and (11), be reduced to the form

$$a_2 = \frac{2n^4(R-1)}{2n^4(R-1)+3}. \quad (12)$$

III. DENSITY-FUNCTIONAL CALCULATIONS: COMPUTATIONAL DETAILS

Density-functional calculations have been carried out on a simplified model chromophore in various configurations as

shown in Figs. 2(a)–2(e). The geometries of the isolated, monomeric chromophore molecule have been fully optimized in configurations where both azo groups adopt a *trans* geometry [Fig. 2(a)], and two more configurations, where only one azo group takes a *trans* geometry [Figs. 2(d) and 2(e)], while the other one takes a nonplanar *gauche* configuration. (Following the usual terminology, this type of *gauche* configuration will nevertheless be labeled *cis*. A local minimum on the molecule's potential energy surface corresponding to a planar *cis*-type configuration has not been found by geometry optimization.) The geometry optimizations have been carried out using the B3LYP exchange-correlation functional [15,16] in combination with a correlation-consistent basis set of polarized double-zeta quality [17]. This approach is known to yield good geometries for organic molecules. The GAUSSIAN 03 program has been used for these calculations [16].

Based on the optimized geometry of the isolated *trans,trans* chromophore [both NN groups of the molecule are in a *trans* state, see Fig. 2(a)], several dimer configurations have been constructed without further geometry optimization. Specifically, configurations in which two chromophore molecules are arranged in a parallel or antiparallel relative orientation are studied at distances of $d=0.3, 0.35,$ and 0.4 nm between the parallel molecular planes of the individual monomer molecules. These simple arrangements of chromophore dimers may be regarded as a very first and crude model to assess the influence of chromophore-chromophore

TABLE I. Chromophore contents c_{chr} , glass transition temperatures T_g , poling temperatures T_{pol} , and Pockels coefficients r_{13} of the materials used.

c_{chr} [mol %]	c_{chr} [wt %]	T_g [°C]	T_{pol} [°C]	r_{13} [pm/V]
20	54	101	106	13.5
30	67	104	114	14.3
40	76	120	122	23.3
60	88	100	110	42.5
100	100	94	102	40.3
100	100	120	110	16.7
100	100	120	116	24.4
100	100	120	118	33.4
100	100	120	128	18.8
100	100	120	135	12.4

interactions on the optical properties. At this stage, no attempts are made to study this effect at a more detailed level, such as modeling of environmental effects or molecular dynamics.

Using this set of monomer and dimer geometries, the optical absorption spectrum is simulated computationally by means of density-functional calculations. To this end, vertical electronic excitation energies and corresponding intensities are calculated within the framework of time-dependent density-functional theory (TD-DFT) [18,19] as implemented into the Amsterdam density functional program (ADF) [20,21]. In calculations of this type, the quality of the one-electron basis set employed on one hand and the choice of the exchange-correlation functional on the other hand constitute two major approximations determining the quality of the results. In this work, an exchange-correlation potential and kernel due to the local density approximation (LDA) is employed in combination with a basis set of polarized double-zeta quality (DZP basis set). It is believed that this level affords a good compromise between accuracy and numerical feasibility for the purpose of the present, qualitative considerations. Errors are expected to range within approximately 0.5 eV for valence excitations of larger molecules such as those studied here using the chosen level of computation. More sophisticated approaches may be used to obtain more quantitative accuracy, at the cost of higher demands in computational resources. However, given the crude model of chromophore clustering assumed in this study (see above), there is no advantage in going beyond the present level of theory here.

IV. EXPERIMENTAL METHODS

A. Material and sample

The polymers investigated are one homopolymer and four copolymers, the synthesis of which can be found in Refs. [22,23]. The homopolymer consists of 100% of the unit shown in Fig. 2(f) which is functionalized with a side-chain bis-azo chromophore and has an averaged molar mass of 11 500. The copolymers are statistically built up by the two monomer units shown in Figs. 2(f) and 2(g). Copolymers

with 20, 40, 60, and 80 mol % of unit f are polymerized with averaged molar masses of 10 500, 12 700, 13 300, and 12 500, respectively. The chromophore shown in Fig. 2(f) has an approximate dipole moment of $\mu=7$ D¹ as estimated by density-functional calculations on the chromophore shown in Fig. 2(a), and a hyperpolarizability $\beta_{zzz}=8.36 \times 10^{-38}$ Vm⁴ measured using hyper-Rayleigh scattering [(SHG), $\lambda=1500 \rightarrow 750$ nm] [24]. The chromophore density has been estimated to $N=1.575 \times 10^{27}$ m⁻³ for the polymer with 100% chromophore content. For the series of the electro-optic and absorption measurements as a function of the poling temperature a fractionated polymer with a higher glass transition temperature (120 °C) is used [25].

The polymers are dissolved in cyclopentanone with a concentration of 100 mg/ml and spin coated onto indium tin oxide (ITO) coated glass plates for a duration of 20 s with rotation speeds of the order of 3000 rpm, which were varied in order to obtain several film thicknesses. The films are dried in an oven at 80 °C for several hours. Typical film thicknesses are 0.5–1.0 μ m measured using a profilometer (Dektak). Then, the films with 100% chromophore content are corona poled [26] at various temperatures (electric field perpendicular to the film plane), while the polymer films with different chromophore concentrations are each corona poled at their individual, previously determined, optimal poling temperature with respect to highest Pockels coefficients (see Table I).

The final step of the sample preparation is the deposition of finger gold electrodes by sputtering on top of the polymer film. This was done by using an aluminum mask leaving some areas transparent for absorption measurements in transmission, while the other areas can be used in the reflection interferometer (see Fig. 3). All electro-optic and dichroism measurements have been performed several times at six to nine different locations on each sample and for each sample the data is averaged.

B. Electro-optic measurements

In order to measure the electro-optic effect, the samples are investigated at room temperature in a free beam Mach-

¹1 D(Debye)=3.336 $\times 10^{-30}$ Cm.

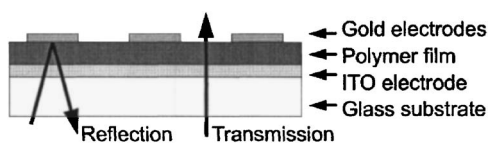


FIG. 3. Sample geometry.

Zehnder interferometer proposed by Norwood, Kuzyk, and Keosian [27]. This technique allows us to determine the components of the Pockels tensor independently. The coefficients are obtained by measuring phase changes due to electric-field-induced refractive index changes and calculating the electric susceptibility. The actual experimental setup, measurement procedure, and calculations are described in greater detail in Ref. [29].

C. Refractive index measurements

For later analysis the spectrum of the refractive index of the material is needed. Therefore two complementary measurements are performed. For the first one a prism coupler (Metricon) is used for waveguide spectroscopy [28]. The refractive index is determined by the transmitted modes in the polymer film to be 1.88 at a wavelength of 685 nm, 1.74 at 1300 nm, and 1.72 at 1550 nm. The values presented are measured in TE mode (polarization in the film plane). The values for the transverse magnetic (TM) mode are around 0.05 smaller due to a slightly anisotropic orientation caused by the spin coating process, while each corona poling procedure induces, again, minor changes. However, because of possible scratches from the prism coupler and resulting short cuts, the measurements cannot be performed for each sample after the spin coating and before the sputtering. Therefore, an unpoled sample is chosen to be used as a reference.

In order to obtain the entire spectrum of the index values from 335 to 2240 nm the measured absorption spectrum of a dilute solution of the polymer in tetrahydrofuran (THF) contained in a cuvette is used. A Varian Cary 500 spectrometer is employed. The absorption coefficient of the bulk material is calculated using the path length within the solution and the polymer concentration. Finally, the Kramers-Kronig relation is applied, an interconnection between the absorption coefficient and the refractive index. A constant offset value has to be added to the spectrum to match the three values of the prism coupler, because the integration is performed over the limited measured region of wavelengths. The result is shown in Fig. 4.

D. Dichroism measurements

For determining the second order parameter the method of linear dichroism is applied [30]. The spectrometer used for investigation is, again, the Varian Cary 500. The absorption of the sample films is measured in transmission and with a beam incidence angle of $\alpha = \pi/4$ with light polarized parallel and perpendicular with respect to the incident plane over a wavelength region from 300 to 800 nm. This range is chosen, because there are significant absorption peaks of the rodlike chromophore side chains, such as those of the photoisomer-

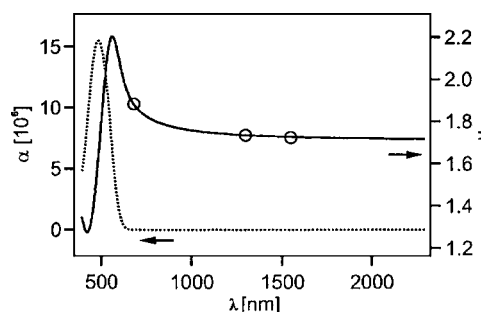


FIG. 4. The absorption coefficient α of the polymer (dotted line) and the refractive index n (solid line) as a function of the wavelength λ . The circles indicate the values measured using the prism coupler.

ization. An ITO-coated glass plate is placed in the reference arm of the spectrometer to correct the according absorption of the substrate. Prior to these measurements, the spectra of the reflectivities of the air-glass, the air-ITO, and the air-polymer interfaces are measured in a modification of the same spectrometer for measurements in reflection mode. They are used to correct the recorded absorption spectra of the polymer films.

E. X-ray scattering

Wide-angle x-ray scattering is measured in a grazing incidence geometry [(GIWAXS), Fig. 5]. Cu $K_{\alpha,\beta}$ radiation is generated by a rotating anode operating at 10 kW and is then focused, collimated, and filtered (only Cu K_{α} is selected) by a multilayer x-ray mirror. Scattering from the sample substrate is suppressed, except from the topmost layers, by setting the sample surface to a very small angle with respect to the x-ray beam [31]. In this manner scattering measurements of nanometer thin films are feasible. The scattered signal was recorded on photostimulable image plates and later scanned. The three samples used in this experiment are made of the polymer with 100% chromophore concentration and a glass transition temperature of 94 °C. The films are poled at 84, 102, (the optimal temperature), and 124 °C.

V. RESULTS

A. Density-functional calculations

Graphs a and b of Fig. 6 show the absorption spectra obtained using density-functional calculations (cf. Sec. III). The calculations only yield peak positions and oscillator

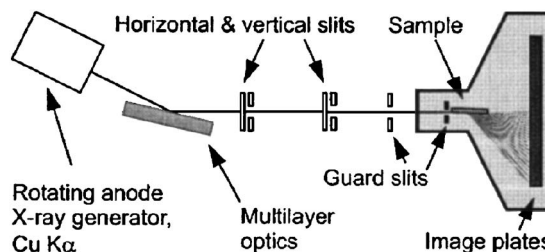


FIG. 5. Grazing incidence wide-angle x-ray scattering setup.

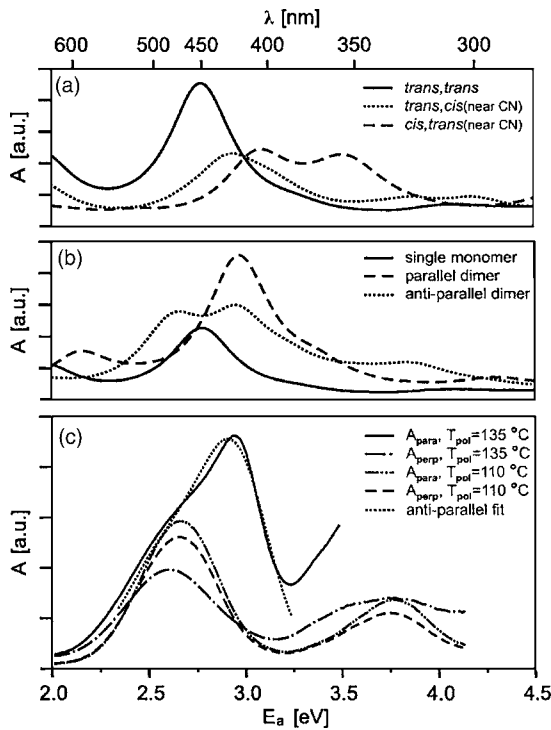


FIG. 6. Spectra of absorption A as a function of the wavelength λ and as a function of the photon energy E_a , all with same scaling; graph a: *trans,trans* chromophore [solid curve; see Fig. 2(a)], of a *trans,cis* chromophore [dotted curve; see Fig. 2(e)], and of a *cis,trans* chromophore [dashed curve; see Fig. 2(d)]; graph b: an isolated single *trans,trans* chromophore (solid, same as in graph a), of a dimer in parallel (head-to-head) orientation [dashed, see Fig. 2(b)], and of a dimer in antiparallel (head-to-tail) orientation [dotted, see Fig. 2(c)]; graph c: material with 100% chromophore concentration poled at 135 °C measured with parallel (solid) and perpendicularly (dash-dotted) polarized light and of the one poled at 110 °C measured with parallel (dash-dot-dotted) and perpendicularly (dashed) polarized light. The dotted line represents a curve fit with the density-functional results of the antiparallel dimer.

strengths (cross sections). For the illustrations, a Lorentzian line broadening with a uniform FWHM (full width at half maximum) of 0.4 eV has been used. The oscillator strengths associated with the excitation energies are computed from the associated transition dipole moment vectors. These vectors are invariably dominated by the z component, which coincides with the principal molecular axis of the chromophores. The computed intensities therefore correspond to experimental spectral intensities measured with polarized photons, the electric field vector of which is parallel to the principal molecular axis. According to the present calculations, the major absorption peak of a single *trans,trans* chromophore has a position around 450 nm. Photochemical *trans/cis* isomerization results in a blueshift of the major absorption lines. A *cis,trans* configuration with the *trans* NN group close to the CN group [Fig. 2(e)] results in a second major peak [now two peaks at about 410 and 360 nm, see Fig. 6(a)], while an isomerization of the other NN bond [Fig. 2(d)] changes the shape of the curve by adding a shoulder for shorter wavelengths (peak at around 430 nm). When two *trans,trans* molecules are placed close to each other the

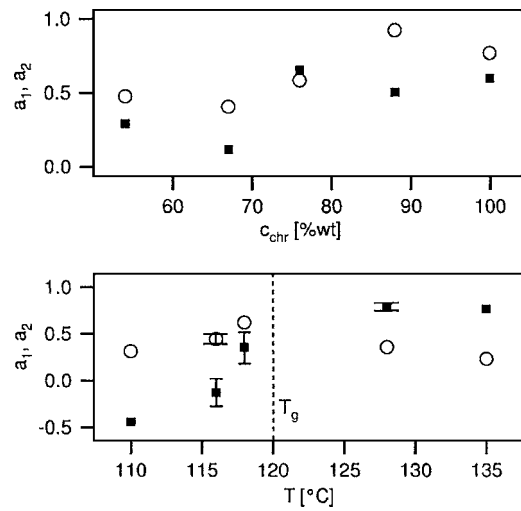


FIG. 7. The first (open circles) and second (filled squares) order parameter a_1 and a_2 as functions of the chromophore concentration c_{chr} (top graph) and as functions of the previous poling temperature T (graph below). T_g marks the glass transition temperature.

change in the calculated absorption spectrum is very small for distances of 0.4 and 0.35 nm or for a skew configuration (data not shown). The two special cases we focus on here are a parallel [head-to-head, Fig. 2(b)] and an antiparallel [head-to-tail, Fig. 2(c)] alignment with a distance of $d=0.3$ nm. In the first case there is one main absorption peak at 420 nm [a shift to shorter wavelengths with respect to an isolated monomer, see Fig. 6(b)] and in the second case there are two major peaks at 470 and at 420 nm.

B. Orientation distribution

The Pockels coefficients measured show the ratio $r_{33}:r_{13} = 3:1$. Assuming the orientated gas model [3], the Pockels coefficients have in fact been shown to follow this relation [32]. Even though higher values have been measured for this ratio [27], the approximation has proved valid for many polymers [33], especially for the ones under investigation in this article [29]. This leads us from the Eqs. (9) and (10) to

$$a_1 = \frac{1}{fN\beta_{zzz}} 5r_{13} \quad (13)$$

and

$$a_3 = 0. \quad (14)$$

The first order parameters, calculated with Eq. (13), are displayed in Fig. 7 as functions of the chromophore concentration (top graph, open circles) and as a function of the poling temperature (graph below, open circles). The first order parameter is lower in materials with low chromophore concentrations, increases until about 90 wt %, and then falls off again for 100%. For the material with 100% chromophore content corona poled at different temperatures the first order parameters rise as the poling temperature increases. However, above the glass transition temperature, the coefficients decrease again. These results are consistent with those in previous publications [29].

Graph c in Fig. 6 shows examples of the absorption spectra of two polymer films, one previously poled well below and the other one well above the glass transition temperature, measured with light of parallel and perpendicular polarization. All spectra show strong absorption for wavelengths between 380 and 600 nm. The sample poled at 135 °C (solid and dash-dotted curve) shows broader peaks than the one poled at 110 °C (dashed and dash-dot-dotted curve). With parallel polarized light, apart from the peak noticed in all other curves at around 470 nm, a second large peak at shorter wavelengths (around 420 nm) appears in the spectrum of the sample poled at high temperature leaving the first one like a shoulder of the curve. One should note that the dichroic ratios of the two samples, calculated by dividing the absorption of parallel polarized light by the absorption of a perpendicular polarized one, are qualitatively inverse to each other.

In the following, the shape of the measured spectrum is described. The density-functional calculations performed provide excitation energies and corresponding oscillator strengths. While the former trivially give information about peak positions, the latter ones correspond to the integral over a peak in an absorption spectrum. Information about the line-width of a peak is not given, since line shapes depend highly on the molecular environment and other influences. Of course, peaks in the measured spectra also occur for wavelengths shorter than 380 nm, but they are not required for evaluation of the orientation of the dipolar side chains, since the absorption peaks under investigation are known to correspond to the rodlike π orbitals of the chromophores. A curve fit is performed of the absorption spectrum measured with parallel polarized light on a film poled at 135 °C [solid curve in Fig. 6(c)], using the calculated line spectrum for an anti-parallel dimer [represented as the dotted curve in Fig. 6(b) with an FWHM of 0.4 eV]. Only the two most pronounced calculated lines are used (actually, two clusters of two and three lines, respectively; one at around 2.62 eV and the other one at around 2.96 eV). While the two peak positions and the ratio of their integrals are kept constant, only the two line-widths (FWHM), and therefore the maxima, are left to be free curve fit parameters. The result is plotted as the dotted curve in graph c in Fig. 6.

The analysis of the absorption data and the calculations of the second order parameters are performed as follows. The dichroic ratio has to be calculated for wavelengths, to which mainly the rodlike chromophores respond. However, for the different samples and the two polarizations, the peaks are at distinct positions with varying amplitudes. Therefore, this cannot be done at a single wavelength. The absorption peaks are integrated over integration windows consisting of the combined full width range of the individual spectra measured with parallel and perpendicularly polarized light at the empirically chosen value of $1/e$ of the peak maximum. Peaks at wavelengths shorter than 400 nm are neglected. Then, the calculations of Eqs. (11) and (12) are done with those values. The results are also shown in Fig. 7. At low chromophore concentrations and at low temperatures, the second order parameters are low, yielding even negative values for low temperatures. As the concentration rises to higher than 70 wt %, higher values for a_2 are obtained. The behavior is even stronger pronounced as the poling temperature is

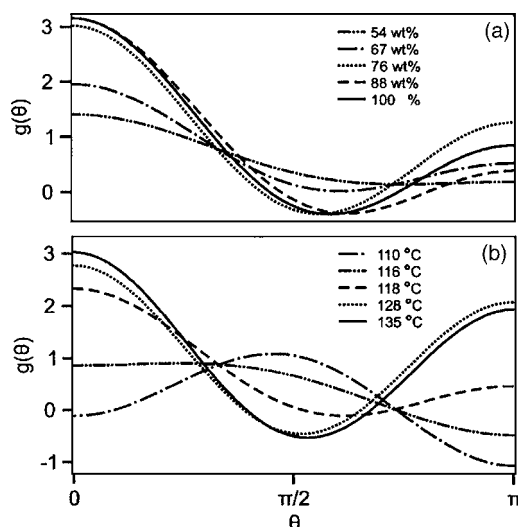


FIG. 8. Chromophore orientation distributions as functions of the polar angle θ ; graph a: polymers with different chromophore concentrations, previously corona poled at each one's individual optimal poling temperature [$g_c(\theta)$]; graph b: a polymer with 100% chromophore concentration previously corona poled at different poling temperatures [$g_T(\theta)$].

increased in the high concentration material having a significant rise from the almost minimal possible to the maximal possible values of a_2 within only a few degrees Celsius.

Subsequently, the orientation distribution functions (ODFs) are calculated using Eq. (2) up to the third order. They are displayed in Fig. 8. In all samples with different chromophore concentrations poled at the optimal temperature with respect to the Pockels coefficient (graph a) more chromophores point into the direction of the externally applied electric field ($\theta=0$) than opposite to it ($\theta=\pi$). However, head-to-tail orientation (neighboring chromophores pointing into the opposite direction) is clearly notable. Even more interesting is the set of curves in graph b. At the lowest temperatures 110 and 116 °C, a peak or a shoulder, respectively, appears at $\theta=\pi/2$. At the highest temperatures, 128 and 135 °C, almost as many chromophores point in the direction of the external electric field as against it.

The error bars displayed in Fig. 7 represent statistical errors. For the first order parameters they are all of the order of 10%. For the second order parameter they depend highly on the magnitude, ranging around 5% for the highest values, but exceeding unity for the small ones (such as for the value at 116 °C poling temperature, see Fig. 7). This is very understandable and due to the fact that the target of the dichroism measurements is to record a very small difference in absorption within a wavelength range, where the material is by many orders of magnitude stronger absorbing than in other wavelength regions. Another reason for the high error values is the specific mathematical kind of interrelation between the experimentally measured properties and the calculated parameters. In special cases, it leads from rather small deviations of the absorption to large ones of the second order parameter. In order to reduce the statistical error for the crucial samples, up to 20 spectra with integration times of several seconds per recorded wavelength are measured and av-

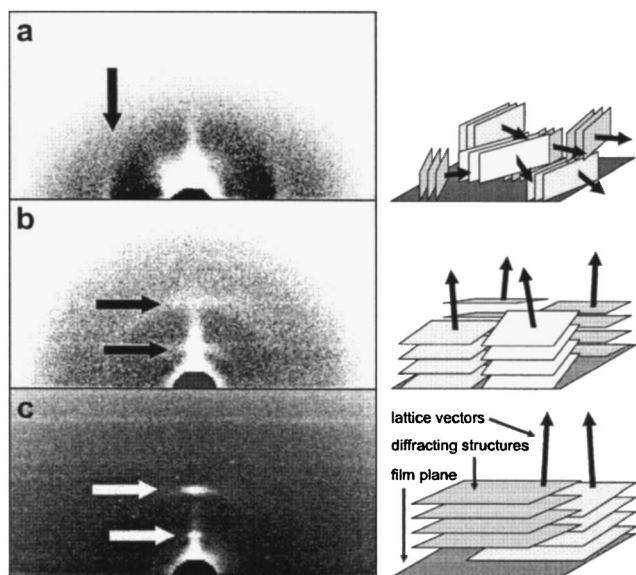


FIG. 9. X-ray scattering images (left) of polymer films with 100% chromophore content and a glass transition temperature of 94 °C poled at 84 °C (graph a), 102 °C (graph b), and 124 °C (graph c). The right column schematically represents according diffracting structures with respect to the horizontal film plane: very small domains with very few diffracting planes and a large angular distribution with in-plane order (a), small domains with few diffracting planes and still a large angular distribution with out-of-plane order (b), and larger domains with more diffracting planes and a small angular distribution, again, with out-of-plane order (c).

eraged. At the same time, the systematic errors of properties, such as the chromophore densities, are very difficult to estimate. The negative values of the orientation distributions, which are physically not meaningful, might be attributed to these systematic errors (see Fig. 8). However, the errors give only an offset to all second order parameters and leave the values still sufficiently accurate to be able to make qualitative comparisons of the different samples.

C. X-ray scattering

In all samples, diffuse scattering from the glass substrate is observed, as well as powder rings from cubic tin-doped indium oxide ITO ($d_{211}=0.413$ nm, $d_{222}=0.292$ nm, $d_{400}=0.253$ nm). Figure 9 shows diffraction patterns of polymer samples corona poled at three different temperatures. Besides the recorded scattering signals, ordering is schematically proposed in the right column of the figure. Graph a shows the scattering from the sample poled at 84 °C, well below glass transition temperature. A phase with in-plane order is observed with a periodicity of 1.35 nm. The scattering signal is not a single peak, but rather broad and very weak, however still detectable. The material is largely disordered. The diffracting structures are small and distributed over a wide angle. Graph b shows the scattered x-ray pattern of a sample, which has been poled at 102 °C (the optimal poling temperature). A phase with out-of-plane order is observed. Again, the diffracted signal does not consist of single peaks, but broad quarter circles implying a distribution of diffracting struc-

tures around a perpendicular position with respect to the film normal. However, the signal is stronger. The positions of the signals correspond to the first- and the second orders of diffraction from these structures with a periodicity of 2.7 nm. The diffracting structures are bigger and, again, distributed over a wide angle. Finally, shown in graph c, the sample poled at 124 °C yields the sharpest peaks, both azimuthal and radial, revealing the highest order, again, out-of-plane with a structure periodicity of 2.7 nm. The diffracting structures are bigger (smaller radial broadness) and more oriented (smaller azimuthal broadness). All graphs are shown with the same scaling. The gray scale has been adjusted suitably for each graph in order to be able to identify the diffraction maxima.

VI. DISCUSSION

By comparing the absorption spectra obtained by density-functional calculations with the measured ones (both in Fig. 6) the following statements can be made: The calculations support the view that the amount of molecules being in a *cis* configuration is either not existent or negligible. All molecules appear to be in a *trans,trans* geometry. At room temperature and at the low light intensity used by the spectrometer this is expected. The case of *cis,cis* configurations is not considered for obvious reasons.

The measured absorption curves for low poling temperatures and those for high poling temperatures measured with perpendicularly polarized light match the single calculated peak of the *trans,trans* molecule with a deviation of about 0.1 eV. The double peak of the anti-parallel alignment cannot be used for the interpretation of those spectra and the single peak of the parallel configuration shows a deviation of more than 0.3 eV. However, a quantitative agreement of the present model calculations with the experimental results should not be assumed. Out of these results one can expect a not so strong dipole-dipole interaction after poling at low temperatures.

The spectrum for high poling temperatures measured with parallel polarized light can be curve fitted surprisingly well with the results of the calculations for antiparallel (head-to-tail) alignment considering that all values used are taken from approximate gas-phase density-functional calculations (peak positions and peak integrals) and only two curve fit parameters (line broadenings) are left free. The broader peak positioned at lower energy (2.62 eV) is now only visible as a shoulder to the main peak at 2.96 eV [see dotted curve in Fig. 6(c)]. Of course, at first glance, the curve fit does not resemble the dotted curve in Fig. 6(b). However, it uses the same calculated line spectrum with the mere difference that now not all peaks have the identical FWHM of 0.4 eV. Since the spectrum of the parallel dimer [dashed curve in Fig. 6(b)] does not contain a major second peak within the wavelength region in question, the necessary shoulder in the measured absorption could not be obtained and the fit (not shown) is substantially worse. Of course, one could also assume the superposition of absorption peaks caused by isolated chromophores and those in parallel orientation. However, there are three reasons why this is probably not appropriate. First of all, the ratio of the integrals of the two major peaks in *all*

spectra measured at high temperatures with parallel polarization match the calculated ones of the antiparallel orientation. Only one, an averaged one, is plotted in this paper. Second, the chromophores are already in a higher energy state when oriented parallel (head-to-head) and favor relaxation toward a random orientation. The force from the dipole-dipole interaction makes an anti-parallel (head-to-tail) dipole orientation rather favorable. And third, there is no obvious reason why the absorption peak of the isolated chromophores broadens when the majority of the chromophores goes into a head-to-head liquid-crystalline phase decreasing the overall disorder in the material. Because of all that, it can be assumed that after poling at a high temperature the majority of the chromophores stick out of the film plane in an antiparallel orientation, not being detected with perpendicular polarized light, giving less absorption [dash-dotted curve in Fig. 6(c)].

The results for the order parameters (Fig. 7) are not entirely as expected. One would think that at low chromophore concentrations the first order parameter must be at least as high as for higher concentrations (top graph, circles), because the dipole-dipole interaction is smaller. This is not observed and we can only speculate about the reasons. All other results are consistent with our intuitive picture: As the poling temperature increases, and therefore the rotational mobility, at first the first order parameter increases, the chromophores can align better in the externally applied electric field. However, at even higher temperatures, the dipole-dipole interaction forces the chromophores into a head-to-tail orientation, forming a liquid crystalline phase, diminishing the inversion symmetry and therefore the first order parameter, while the second order parameter increases steadily. An increasing amount of chromophores in antiparallel arrangement can also be seen for higher chromophore concentrations, where dipole-dipole interactions also increase the second order parameter.

Figure 8 displays the orientation distribution functions. The results confirm the idea. After spin coating the chromophores lay largely disordered still with a broad distribution in the film plane ($\theta = \pi/2$) (lowest temperature in graph b). In fact, the ordering of side groups can be attributed to the mechanical features of the spin coating process itself. This effect has been investigated for other polymers and various film thicknesses [35] by, for example, comparing orientation in spin coated films with the one in Langmuir-Blodgett films [36]. As expected, the anisotropy vanishes when the film is heated up to the glass transition region of the material [37]. Poling at high enough temperatures increases the orientation along the field ($\theta = 0$), while still keeping opposite orientation ($\theta = \pi$) low. Increasing the rotational mobility at higher poling temperatures makes a second peak against the field appear. The strong dipole-dipole interaction leads to crystalline head-to-tail orientation. Choosing the optimal distributions for different chromophore concentrations with respect to the electro-optic response (graph a), there is a tradeoff between obtaining the largest response by increasing the chromophore concentration and decreasing it, when the dipole-dipole interaction dominates.

It should be mentioned that the cooperative movements and the high chromophore density may exhibit a large birefringence in the material. Additionally, the chromophores are

not cylindrically symmetric. These two properties can, in fact, result in a nonuniaxiality of the orientation distribution. This biaxial orientation, where the dependence on the azimuthal angle ϕ cannot be neglected anymore, has been investigated in other photoaddressable bisazo polymers [34].

Finally, the attention is drawn to the complementary x-ray scattering (Fig. 9). The results reveal that it cannot be the chromophores diffracting the x-rays, but presumably the backbones of the polymers or just planes of oriented chromophores laying side by side and having higher electron densities than interplane space. One can estimate the length of the representative monomer to be of the order of just below 2.0 nm. In combination with the derived values from the x-ray scattering, predictions about the diffracting element can only be speculations. However, with the space, which the polymer backbone occupies, and an intermolecular distance of the order of 0.3 nm, one reaches, in fact, a value of 2.7 nm for a distance of diffracting planes possibly consisting of the polymer main chains while the side chains act as spacers. In such a constellation, these side chains attached to one polymer main chain could point atactic in opposite directions and alternate antiparallel with every other side chain of the adjacent polymer molecule in order to form the liquid crystalline phase. Comparing the orientation distribution functions for different poling temperatures [Fig. 8(b)] with the schemes drawn from the x-ray scattering results (Fig. 9), both give precisely the same information about order in the material. Order, in this sense, can be associated with the number of diffracting planes within single domains and the angular distribution of the domains' orientation (schematically displayed in the right column of Fig. 9), observed as the sharpness of a peak or line in the recorded diffraction diagram. First, the highest order is obtained at the highest temperatures (with many planes parallel to the film plane). Second, at medium temperatures the order gets less pronounced (fewer diffracting planes, broader angular distribution), while the orientation of the order keeps the same (still with order out of the film plane). Third, leaving the material largely disordered, at the low temperatures the order is even much less pronounced (even fewer diffracting planes) and perpendicular to the ones in the other two cases (diffracting planes perpendicular to the film plane, that is in-plane order). It is puzzling that the periodicity of the diffracting structures differs between the lowest temperature and the other two. The center in Fig. 9(a) is blurred and a first diffraction order of possible structures with a periodicity of 2.7 nm cannot be detected even though it might be there. Furthermore, the diffracting distances have precisely a ratio of 2. This can indicate that, in the highly ordered material, a different phase builds up. An example for such a change is a crystallization in a centered unit cell. Thus, the intermolecular packing distance would be still the same. However, the axis' periodicity is effectively doubled.

VII. CONCLUSION

Combining electro-optic and linear dichroic absorption measurements, density-functional calculations, and grazing incidence wide-angle x-ray scattering, conclusions for the

influence of dipole-dipole interaction on the orientation distribution in high chromophore density electro-optic photoaddressable polymers can be consistently drawn: As mobility or concentration rise the largely disordered material with the chromophores laying in the film plane after the spin coating process reaches higher order in the direction of the poling field with a head-to-tail orientation of the chromophores that becomes more and more pronounced for higher chromophore concentrations and poling temperatures finally reaching a liquid crystalline phase.

ACKNOWLEDGMENTS

We thank R. Hagen and S. G. Kostromine from BAYER Material Science AG for providing the material. Furthermore, we thank E. Soergel for helpful discussions. W.H. gratefully acknowledges support in form of a Marie Curie European Reintegration Grant within the 6th European Community RTD Framework Programme and a grant of computer time from the John von Neumann Institute in Jülich.

-
- [1] M. Lee, H. E. Katz, C. Erben, D. M. Gill, P. Gopalan, J. D. Heber, and D. J. McGee, *Science* **298**, 1401 (2002).
- [2] H. Ma, A. K.-Y. Jen, and L. R. Dalton, *Adv. Mater. (Weinheim, Ger.)* **14**, 1339 (2002).
- [3] J. W. Wu, *J. Opt. Soc. Am. B* **8**, 142 (1991).
- [4] R. D. Dureiko, D. E. Schuele, and K. D. Singer, *J. Opt. Soc. Am. B* **15**, 338 (1998).
- [5] T. G. Pedersen, K. Jespersen, P. M. Johansen, and J. Wyller, *J. Opt. Soc. Am. B* **19**, 2622 (2002).
- [6] K. G. Jespersen, T. G. Pedersen, and P. M. Johansen, *J. Opt. Soc. Am. B* **20**, 2179 (2003).
- [7] R. Hagen and T. Bieringer, *Adv. Mater. (Weinheim, Ger.)* **13**, 1805 (2001).
- [8] F. I. Mopsik and M. G. Broadhurst, *J. Appl. Phys.* **46**, 4204 (1975).
- [9] C. J. F. Böttcher, ed., *Theory of Electric Polarization*, Vol. 1 (Elsevier Scientific Publishing Company, Amsterdam, 1973).
- [10] J. F. Nye, ed., *Physical Properties of Crystals* (Clarendon Press, Oxford, 1985).
- [11] S. Lopes, M. X. Fernandes, M. Prieto, and M. A. R. B. Castanho, *J. Phys. Chem. B* **105**, 562 (2001).
- [12] B. Nordén, G. Lindblom, and I. Jonáš, *J. Phys. Chem.* **81**, 2086 (1977).
- [13] L. B.-Å. Johansson, Å. Davidsson, G. Lindblom, and B. Nordén, *J. Phys. Chem.* **82**, 2604 (1978).
- [14] L. B.-Å. Johansson, and Å. Davidsson, *J. Chem. Soc., Faraday Trans. 1* **81**, 1375 (1985).
- [15] A. D. Becke, *J. Chem. Phys.* **98**, 5648 (1993).
- [16] M. J. Frisch *et al.*, ed., *GAUSSIAN 03* (Gaussian, Inc., Pittsburgh, Pennsylvania, 2003).
- [17] T. H. Dunning, Jr., *J. Chem. Phys.* **90**, 1007 (1989).
- [18] E. Runge and E. K. U. Gross, *Phys. Rev. Lett.* **52**, 997 (1984).
- [19] M. E. Casida, *Recent Advances in Density Functional Methods*, edited by, D. P. Chong., Vol. 1 (World Scientific, Singapore, 1995).
- [20] G. te Velde, F. M. Bickelhaupt, E. J. Baerends, C. Fonseca Guerra, S. J. A. van Gisbergen, J. G. Snijders, and T. Ziegler, *J. Comput. Chem.* **22**, 931 (2001).
- [21] S. J. A. van Gisbergen, J. G. Snijders, and E. J. Baerends, *J. Chem. Phys.* **109**, 10644 (1998).
- [22] R. Hagen, T. Bieringer, S. Kostromine, and H. Berneth, German Patent No. 2,003,049,549, A1 (2001)
- [23] H. Berneth, T. Bieringer, R. Hagen, and S. Kostromine, German Patent No. 2,003,113,664, A1 (2003).
- [24] G. J. T. Heesink, A. G. T. Ruiter, N. F. van Hulst, and B. Bölger, *Phys. Rev. Lett.* **71**, 999 (1993).
- [25] R. P. Bertram, N. Benter, D. Apitz, E. Soergel, and K. Buse, *Phys. Rev. E* **70**, 041802 (2004).
- [26] M. A. Mortazavi, A. Knoesen, S. T. Knowel, B. G. Higgins, and A. Dienes, *J. Opt. Soc. Am. B* **6**, 733 (1989).
- [27] R. A. Norwood, M. G. Kuzyk, and R. A. Keosian, *J. Appl. Phys.* **75**, 1869 (1994).
- [28] R. Ulrich and R. Torge, *Appl. Opt.* **12**, 2901 (1973).
- [29] R. P. Bertram, E. Soergel, H. Blank, N. Benter, and K. Buse, *J. Appl. Phys.* **94**, 6208 (2003).
- [30] M. A. R. B. Castanho, S. Lopez, and M. Fernandes, *Spectroscopy (Amsterdam)* **17**, 377 (2003).
- [31] J. Als-Nielsen and D. McMorrow, *Elements of Modern X-Ray Physics* (Wiley, Chichester, 2000).
- [32] K. D. Singer, M. G. Kuzyk, and J. E. Sohn, *J. Opt. Soc. Am. B* **4**, 968 (1987).
- [33] K. D. Singer, M. G. Kuzyk, W. R. Holland, J. E. Sohn, S. J. Lalama, R. B. Comizzoli, H. E. Katz, and M. L. Schilling, *Appl. Phys. Lett.* **53**, 1800 (1988).
- [34] T. Buffeteau, F. Lagugné Labarthe, C. Sourisseau, S. Kostromine, and T. Bieringer, *Macromolecules* **37**, 2880 (2004).
- [35] H. Mensinger, M. Stamm, and C. Boeffel, *J. Chem. Phys.* **96**, 3183 (1997).
- [36] I. Pelletier, I. Laurin, T. Buffeteau, B. Desbat, and M. Pézolet, *Langmuir* **19**, 1189 (2003).
- [37] W. H. Kim, B. Bihari, R. Moody, N. B. Kodali, J. Kumar, and S. K. Tripathy, *Macromolecules* **28**, 642 (1995).